Geophysical and Astrophysical Convection, pp. 00-00
Gordon and Breach Science Publishers

ASTROPHYSICAL CONVECTION AND DYNAMOS

AXEL BRANDENBURG[1], ÅKE NORDLUND[2] and ROBERT F. STEIN[3]

[1] *Department of Mathematics*
University of Newcastle upon Tyne NE1 7RU, UK
[2] *Copenhagen University Observatory*
Juliane Maries Vej 30, DK-2100 Copenhagen Ø, Denmark
[3] *Department of Physics and Astronomy*
Michigan State University, East Lansing, MI 48824

Convection can occur in various astrophysical settings. In this review some aspects of solar convection are highlighted. In deeper layers of the solar convection zones rotation becomes important and can lead to effects such as downward pumping of vorticity and magnetic fields. Rotation has the tendency to partially evacuate vortex tubes making them lighter. This effect can sometimes reverse the core of a downdraft and make it buoyant. The problem of different thermal and dynamical timescales is addressed and finally the formation of magnetic structures by convection is discussed.

1 Introduction

In astrophysics convection can occur in various settings. Convection in stars is ubiquitous. In stars of mass $M \lesssim 2M_\odot$ ($1\,M_\odot \approx 2 \times 10^{33}$ g is the mass of the sun) convection occurs in the outer layers of the star because the gas becomes relatively opaque. At the surface of the sun this convection is manifested by the granulation (Bray et al. 1984), which is a time-dependent cellular pattern similar to classical Rayleigh-Benard convection, such as may be seen by heating a shallow container of oil mixed with aluminum powder as tracer. A comparison with such a kitchen experiment is misleading, however, because it suggests that solar convection is a rather viscous phenomenon. While it is actually true that the viscosity of the gas in the sun (mostly hydrogen and helium) is comparable with that of honey (something like 10^2 cm^2/ s), the Reynolds numbers $\mathrm{Re} = UL/\nu$ are in fact rather large, because of the large length scales L. It is indeed quite typical for astrophysical bodies that such dimensionless numbers take astronomically large values. The Rayleigh number, for example, is around 10^{24} or larger, but we will come back to this below. Before that, let us discuss other examples of astrophysical convection.

Shallow surface convection zones also occur in white dwarfs, one of the end products of stellar evolution of stars with mass less than about eight solar masses. The end products of stars with larger mass are often neutron stars, the remnants of supernova explosions. Just

after a neutron star has formed convection may occur for a very short period of time of a few seconds (see e.g. Thompson & Duncan 1993).

A the typical (local) turnover time is

$$\tau_{\rm turnover} = H_p/u_t. \tag{1}$$

Here, $H_p = |d\ln P/dr|^{-1}$ is the local pressure scale height, and u_t is the turbulent root-mean-square velocity. In solar like stars this ranges from minutes near the surface to months near the bottom. In neutron stars and white dwarfs the typical turnover times are more like $1-10$ ms. The integrated turnover time is

$$t_{\rm turnover} = \int \frac{dr}{u_t(r)} \ . \tag{2}$$

For the sun, which has a rather deep convection zone (30% by radius, or 200 Mm), this is around a month.

The outer layers of stars of mass $\geq 2M_\odot$ are stably stratified, except for very shallow outer convection zones associated with the ionization zones of hydrogen and helium, but stars more massive than $1-2M_\odot$ have convective cores due to high temperature gradients arising from the high temperature sensitivity of nuclear reactions that become possible for stars hotter than the sun.

The energy source of convection is not always nuclear energy. In galaxies, a rather different type of convection occurs. Although galaxies are on average stably stratified, isolated events like supernova and superbubble explosions (collective supernova explosions triggering each other) lead to buoyant outflows. Those events heat the gas locally to 10^6 K, leading to buoyant bubbles that shoot through the gaseous galactic disc into the outer halo. Here the typical dimensions are kiloparsecs, where $1\,{\rm kpc} = 3\times10^{21}$ cm or 3000 light years.

Convection also occurs in another important class of objects – accretion discs – where the source of energy is gravitational potential energy. Matter gradually spirals onto a central object, which could be a protostar or stellar remnant (white dwarf, neutron star, black hole), or it could be a supermassive black hole of 10^8 solar masses or more. In the absence of friction matter would just stay in the same orbit, like the particles in Saturn's rings, and there would be no accretion onto the central object. It is only due to turbulent friction and magnetic fields that matter loses angular momentum. Associated with this is a conversion of potential energy into heat via viscous and Joule heating. This is a remarkable point. Although in astrophysics the microscopic viscosity ν and magnetic diffusivity η are generally very small (in the sense of huge Reynolds numbers), this does not imply that the total viscous and Joule dissipation are necessarily small.

One of the corner stones of Kolmogorov (1941) scaling in turbulence is that the average dissipation is of the order of $\rho U^3/L$, and does not depend on the value of the molecular viscosity. A similar result has recently been demonstrated for magnetic dissipation in driven, low-beta plasmas, where the dissipation scales as $B^2UL/L_{\rm B}^2$, $L_{\rm B}$ being the characteristic length of the field lines (Galsgaard & Nordlund 1996). In accretion discs, turbulent viscous and Joule dissipation can be extremely important. For instance, the most luminous objects in astrophysics are quasars, quasi-stellar objects, which are now believed to be gigantic accretion discs around supermassive black holes, where the source of radiation is viscous and Joule dissipation. So, although viscosity and magnetic diffusion may be "negligibly small", they cannot be neglected and may well be energetically very important. If convection occurs in accretion discs, it is probably not the main source of turbulence.

We conclude this introduction to the rather broad range of astrophysical convection by mentioning a few references. The extent and location of stellar convection zones is described in Kippenhahn & Weigert (1990). Gas flows and related magnetic fields in galaxies are described in Ruzmaikin et al. (1988), and the topic of accretion discs is introduced in the book by Frank et al. (1992). In the following we focus on solar convection.

2 Deep solar convection

In solar convection the Reynolds number, $R_e = UL/\nu$, is very large. The kinematic viscosity ν rises from about $1\,\mathrm{cm}^2/\,\mathrm{s}$ near the surface to about $10^4\,\mathrm{cm}^2/\,\mathrm{s}$ in deeper layers (due to radiative viscosity, i.e. momentum exchange by photons; e.g. Kippenhahn & Weigert 1990). The typical velocities U and vertical scale heights vary from 1 km/s and 1 Mm (= 1000 km) near the surface to 0.1 km/s and 100 Mm deeper down, so the Reynolds number is then roughly

$$\mathrm{Re} = \frac{UL}{\nu} \approx \frac{10^5\,10^8}{1} ... \frac{10^4\,10^{10}}{10^4} = 10^{13} ... 10^{10}. \tag{3}$$

The Peclet number, $\mathrm{Pe} = UL/\chi$, that compares advective effects to thermal diffusion effects, is also very large. Thermal conduction is quite unimportant. Instead there is radiative diffusion of photons, whose mean free path is much larger than that of the electrons. Radiative diffusion can be described by Fick's law, so the radiative flux is

$$\boldsymbol{F}_{\mathrm{rad}} = -K(\rho, T)\boldsymbol{\nabla} T. \tag{4}$$

The radiative conductivity K depends strongly on density ρ and temperature T. In the deeper parts of the solar convection zone most of the opacity is due to close encounters of free electrons passing nearby an ion. This can absorb and emit radiation (free-free transition), and the opacity can be described by a power law (Kramers' opacity), so K is then

$$K = K_0 \left(\frac{\rho}{\rho_0}\right)^{-2} \left(\frac{T}{T_0}\right)^{6.5}. \tag{5}$$

The value of K_0 is well known ($K_0 = 5 \times 10^{-27}\,\mathrm{erg\ cm^{-1}\ s^{-1}\,K^{-1}}$, where $\rho_0 = 1\,\mathrm{g/\,cm^3}$ and $T_0 = 1\,\mathrm{K}$). In the following, however, we shall refer to Kramers' opacities even when the value of K_0 is modified (see below). K increases by about $\sim 10^2$ from the top to the bottom of the convection zone, so the radiative flux increases gradually towards the bottom of the convection zone (the temperature gradient is roughly constant), and takes over completely from convection in the radiative layers below the convection zone. Here, the further increase in conductivity is compensated for by a decrease in the temperature gradient (and a decrease in the surface area), to keep the total luminosity constant.

The radiative diffusivity coefficient, that characterizes the diffusion of temperature perturbations, is

$$\chi = \frac{K}{\rho c_p}, \tag{6}$$

where c_p is the specific heat at constant pressure. The factor ρc_p, the thermal energy per unit mass and Kelvin, increases by about five orders of magnitude through the convection zone (in the surface layers c_p is enhanced by about one order of magnitude relative to an ideal gas). Thus, the rate at which temperature fluctuations are smoothed out by diffusion *decreases* by about three orders of magnitude from the top to the bottom of the convection

zone. Near the bottom of the solar convection zone χ is around $10^7\,\mathrm{cm}^2/\,\mathrm{s}$, so the Peclet number is

$$\mathrm{Pe} = \frac{UL}{\chi} \approx \frac{10^4\,10^{10}}{10^7} \sim 10^7, \tag{7}$$

whereas near the surface typical values based on Kramers' opacity are

$$\mathrm{Pe} \approx \frac{10^5\,10^8}{10^{10}} \sim 10^3. \tag{8}$$

Additional opacity in the surface layers, in particular from the negative hydrogen ion, increases the actual Peclet number there considerably.

It is worth noting that one may write the Peclet number as

$$\mathrm{Pe} = \frac{UL}{K/(\rho c_p)} = \frac{\rho c_p U \delta T}{KT/L}\frac{T}{\delta T} \approx \frac{F_{\rm conv}}{F_{\rm rad}}\frac{1}{\delta \ln T}; \tag{9}$$

i.e., as the ratio of the convective and radiative fluxes, divided by the relative temperature fluctuation. Near the surface, $\delta \ln T \sim 1$, but the radiative flux is only a tiny fraction of the total flux. Near the bottom, $F_{\rm rad} \sim F_{\rm conv}$, but $\delta \ln T \sim 10^{-6}$.

Thus, for both the momentum and the energy equation, it is clear that the real diffusive effects are much smaller than what can be handled by direct numerical simulations, even though the situation is less extreme in the energy equation. The ratio of the diffusion coefficients in the momentum or energy equations is the Prandtl number,

$$\mathrm{Pr} = \nu/\chi = \mathrm{Pe}/\mathrm{Re} \sim 10^3/10^{13}...10^7/10^{10} \sim 10^{-10}...10^{-3} \tag{10}$$

At this point there is a crucial decision to be made. One can either resort to some kind of subgrid scale modeling, or one can use scaled values for the viscosity and the radiative diffusivity, trying to preserve a reasonably small value for the Prandtl number, even though it is clear that one cannot come (even in a logarithmic sense) near solar values. Subgrid scale models, on the other hand, are normally insensitive to the value of Pr and resemble more the conditions for Prandtl number equal unity.

We have taken the attitude that on scales that can be resolved by the simulations, diffusive effects do not depend on the actual values of the microscopic diffusion coefficients, consistent with the Kolmogorov assumption mentioned earlier. Effects due to small Prandtl numbers are then expected only in the range of scales where diffusion of momentum is turbulent, but thermal diffusion is not. In the next section, we briefly mention some effects that may be expected there.

3 Low Prandtl number effects

The importance of the Prandtl number has been emphasized in the context of laboratory convection, but not so much in the context of astrophysical convection. There is one qualitative aspect that arises due to a small value of the Prandtl number. Small Prandtl number means that radiative diffusion is large compared with viscosity. The viscosity determines the typical scale of vortex tubes (Constantin et al. 1995), so a small Prandtl number means that the temperature will rapidly equilibrate across such vorticity structures. The pressure is reduced inside vortex tubes, in proportion to the square of the speed of rotation. Using now the equation of state for a perfect gas,

$$p = \frac{\mathcal{R}T}{\mu}\rho, \tag{11}$$

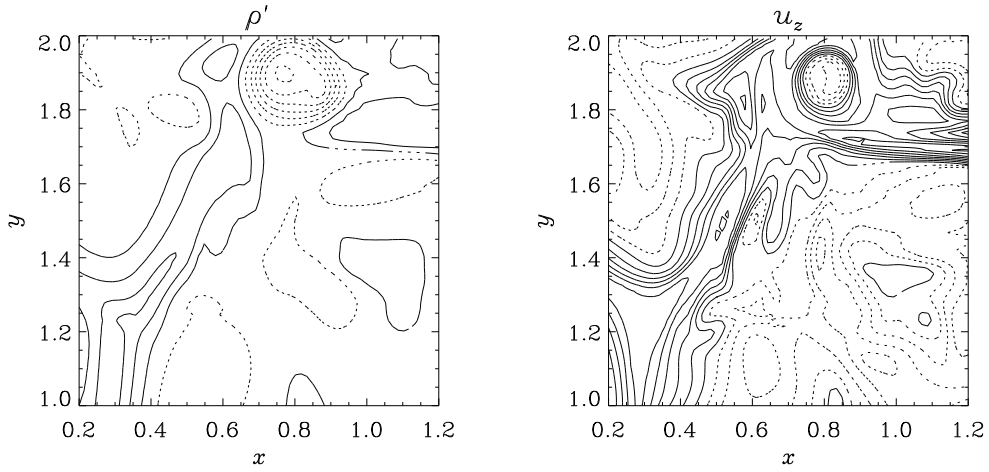

Figure 1: Contours of horizontal slices (just below the surface, $z = 0.1$) of the density fluctuation $\rho' = \rho - \langle\rho\rangle$ (dotted contours mean lighter material and solid contours heavier material) and the vertical velocity u_z (dotted contours mean upward, solid contours downward flow). The downdraft lanes are characterized by $\rho' > 0$ and $u_z > 0$, except in the vortex near the top of the figure, where $\rho' < 0$ (vortex buoyancy) and a small region with $u_z < 0$ has developed. Run D of Brandenburg et al. (1996).

where $\mathcal{R}$ is the universal gas constant and μ the mean molecular weight, we see that for almost uniform temperature across the tube, the density in the tube must be lowered. This has consequences for convective downdrafts, that will be explained next.

First we need to emphasize that, because of vertical density stratification, the area occupied by the convective downdrafts is smaller than the area of the upwelling motions. This is simply because a fluid parcel contracts as it descends and it expands as it ascends. In order to conserve mass ($\rho v S = \text{const}$), the downdrafts have to speed up (their cross-sectional area S decreases, so the velocity v increases); see Stein & Nordlund (1989). This, together with the Coriolis force, sets them into rapidly swirling motion. This is all not very surprising and quite similar to geophysical convection. Also, what does it have to do with small Prandtl numbers? In fact, in what we said above there seems to be a contradiction as to whether the density in the downdrafts is large or small. We started by saying that the density has to be small, because vortex tubes have low pressure. On the other hand, what generates those rapidly spinning downdrafts in the first place is of course the fact that they are cool and therefore dense, so the density cannot be low. This can be understood by considering the following sequence of events: material at the surface cools, becomes dense and begins to descend. As it descends, it contracts and is set into spinning motion. The spinning downdrafts then tend to eject material centrifugally, so the pressure is lowered, relative to what it would otherwise be. If the corresponding density reduction is larger than the density enhancement associated with the downdraft, the buoyancy may actually reverse, and eventually cause also the vertical velocity to reverse. This process has indeed been observed in numerical simulations of low Prandtl number convection in the presence of rotation (Brandenburg et al. 1996, Brummel et al. 1996; see also Fig. 1).

If the Prandtl number were of order unity this process would have been less pronounced,

because the temperature would have been able to adjust to the smaller adiabatic value, so the density reduction would have been smaller by a factor γ.

4 The entropy gradient

In ordinary Boussinesq convection the degree of instability is characterized by the Rayleigh number

$$\mathrm{Ra} = \frac{H^4}{\nu\chi}(\boldsymbol{g}\cdot\boldsymbol{\nabla}\ln T)_0, \tag{12}$$

where the subscript 0 refers to the (unstable) nonconvective hydrostatic state, which is sometimes also the initial state used in simulations. Here, T is the temperature, H the height of the layer, and $\boldsymbol{g}$ is the gravitational acceleration. (Normally one would write $\alpha\boldsymbol{\nabla}T$ instead of $\boldsymbol{\nabla}\ln T$, where α is the expansion coefficient, but for a perfect gas $\alpha = 1/T$; see Chandrasekhar 1961.) This definition is readily extended to the regime of stratified convection by replacing the logarithmic temperature by the normalized specific entropy s/c_p, so

$$\mathrm{Ra} = \frac{H^4}{\nu\chi c_p}(\boldsymbol{g}\cdot\boldsymbol{\nabla}s)_0, \tag{13}$$

where $s/c_p = \ln T - (1-1/\gamma)\ln p$ is the normalized specific entropy, $(\boldsymbol{\nabla}s)_0$ is the entropy gradient of the unstably stratified nonconvective hydrostatic solution and c_p is the specific heat at constant pressure. For a perfect monoatomic gas, $c_p = \frac{5}{2}\mathcal{R}/\mu$.

In the inviscid limit, $\nu \to 0$, stability is simply governed by the sign of $\boldsymbol{g}\cdot\boldsymbol{\nabla}s$. In astrophysics this is known as Schwarzschild's criterion,

$$\boldsymbol{g}\cdot\boldsymbol{\nabla}s > 0 \quad \text{(instability)}. \tag{14}$$

Let us now look at the profile of the horizontally averaged entropy, $\langle s\rangle$, as a function of z using data of a simulation. In Fig. 2 we show the entropy profile from a simulation where Kramers' opacity law is used. The vertical scale in the figure does not accurately represent the sun, especially near the surface which has artificially been pulled further down into the convection zone relative to the sun.

There are basically five regimes; see Fig. 2. The first regime (below 470 Mm) is the stably stratified radiative interior where the average entropy (here normalized by c_p/g) rises at a rate

$$-\boldsymbol{g}\cdot\boldsymbol{\nabla}\langle s/c_p\rangle \equiv N_{\rm BV}^2 > 0, \tag{15}$$

where $N_{\rm BV}$ is the Brunt-Väisälä frequency if the stratification were isothermal. (Because of temperature stratification the actual Brunt-Väisälä frequency is somewhat different.) Between 470 and 500 Mm (regime II) there is another layer where $N_{\rm BV}^2$ is almost unchanged, but the convective flux is now negative. Here are only sporadically entering plumes from the convection zone above that stir up the gas. In regime III (500–540 Mm) $N_{\rm BV}^2$ is still positive, but much smaller than in the deep radiative interior. This regime should be considered as part of the convection zone, because there is a convective flux that is directed upwards. However, according to Schwarzschild this entire layer is still stable. At some point in the middle of the convection zone there is a point (near 540 Mm) where $N_{\rm BV}^2$ finally turns negative and its magnitude increases until one reaches the surface layers (near 690 Mm in the plot), where there is a sharp increase of the entropy. This is then the fifth regime which

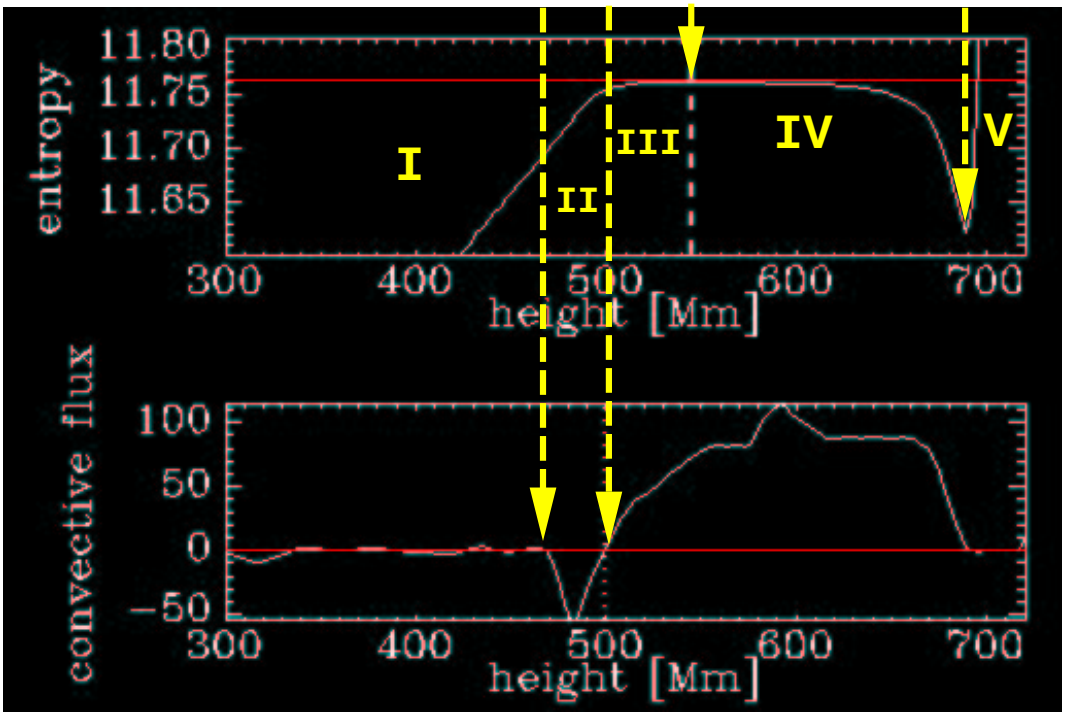

Figure 2: Profiles of entropy and convective flux in a single snapshot of the simulations with Kramers' opacities. Region I is the radiative interior, II the overshoot layer, III the radiative heating layer, IV the bulk of the convection zone, and V the surface layer.

is a stably stratified overshoot layer above the convection zone. Here, $N^2_{\rm BV}$ is again positive and its value is larger than the value for the radiative interior.

To appreciate the properties of the slightly stable profile of $\langle s \rangle$ in the lower part of the convection zone (region III) we should first point out that in simulations with fixed vertical profiles of the conductivity, $K = K(z)$, having a narrow transition region between stable and unstable layers, this regime is very narrow. In Fig. 3 we show the profile of $\langle s \rangle$ from a snapshot of a simulation of Brandenburg et al. (1996), where there are three layers with different values of the conductivity $K = K(z)$. The unstable hydrostatic reference solutions have different polytropic indices in the three regions, with a continuous but rather abrupt change from region to region. As a consequence, the transition from transport by radiation to transport by convection is more abrupt than in the case with Kramers' opacity (Fig. 2).

The existence of a region with positive convective flux but stable average stratification is intimately related to the transition from radiative to convective energy transport (Nordlund et al. 1996). The decrease of the radiative energy flux with radius implies a negative divergence of the radiative energy flux, corresponding to heating of the fluid. Of course, the increase of the convective flux with radius corresponds to a cooling that, on the average, balances the heating from the decrease of the radiative flux. However, the heating and cooling have quite different horizontal distributions, and only cancel when averaged over horizontal area (and time). The radiative flux is approximately uniform, being proportional to the temperature gradient of a medium with very small relative temperature fluctuations. The

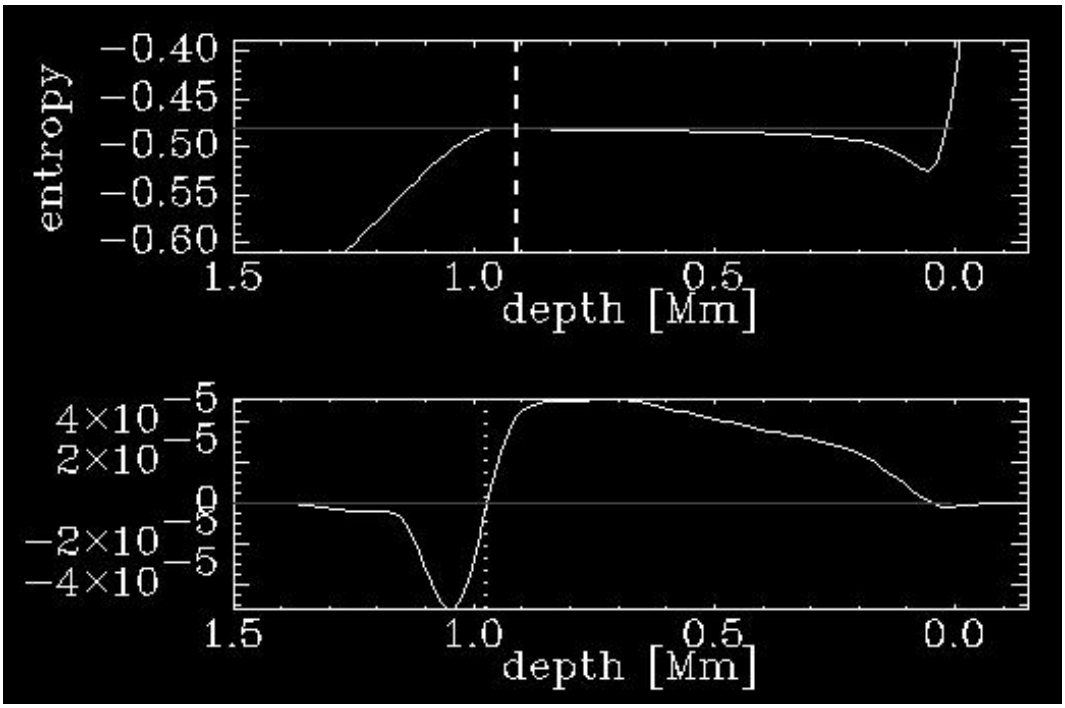

Figure 3: Profiles of entropy and convective flux in a single snapshot of the simulations with fixed piecewise constant conductivity $K(z)$.

convective flux is very non-uniform, being carried mostly by localized, cool downdrafts.

On the background of these considerations, it is easy to understand the reason why the average stratification must be weakly stable in this region (regime III in Fig. 2). The nearly uniform positive heating from the decreasing radiative flux gradually increases the entropy of the ascending material. Cool downdrafts that penetrate into this weakly stable region are decelerated and also gradually loose their entropy contrast relative to the background. In order to penetrate all the way through region III, they must arrive with a sufficient entropy deficiency and/or excess momentum. The gradually decreasing convective flux with depth is the horizontally averaged manifestation of both the decreasing entropy contrast of those downdrafts that manage to penetrate, and the decreasing number of downdrafts that succeed.

In Fig. 4 we show the evolution of two plumes in two different vertical slices of the entropy for the run described in Fig. 2 (i.e. the run with Kramers' opacity). The boundaries between regions II, III, and IV are marked by dotted and dashed lines, respectively. Two different types of plumes are visible: one that plunges down through the entire convection zone into the stable layer below and another that develops a typical mushroom shaped head. The extent of plume penetration is an important problem that needs further investigation.

Figure 5 shows horizontal images of the temperature in four selected layers. Around the upper entropy minimum near the surface ($z = 683\,\mathrm{Mm}$) there is a clear granulation-like pattern with cool downdraft lanes between warm upwellings. This is qualitatively similar to the solar granulation, but here in the model the stratification is less than in reality, so

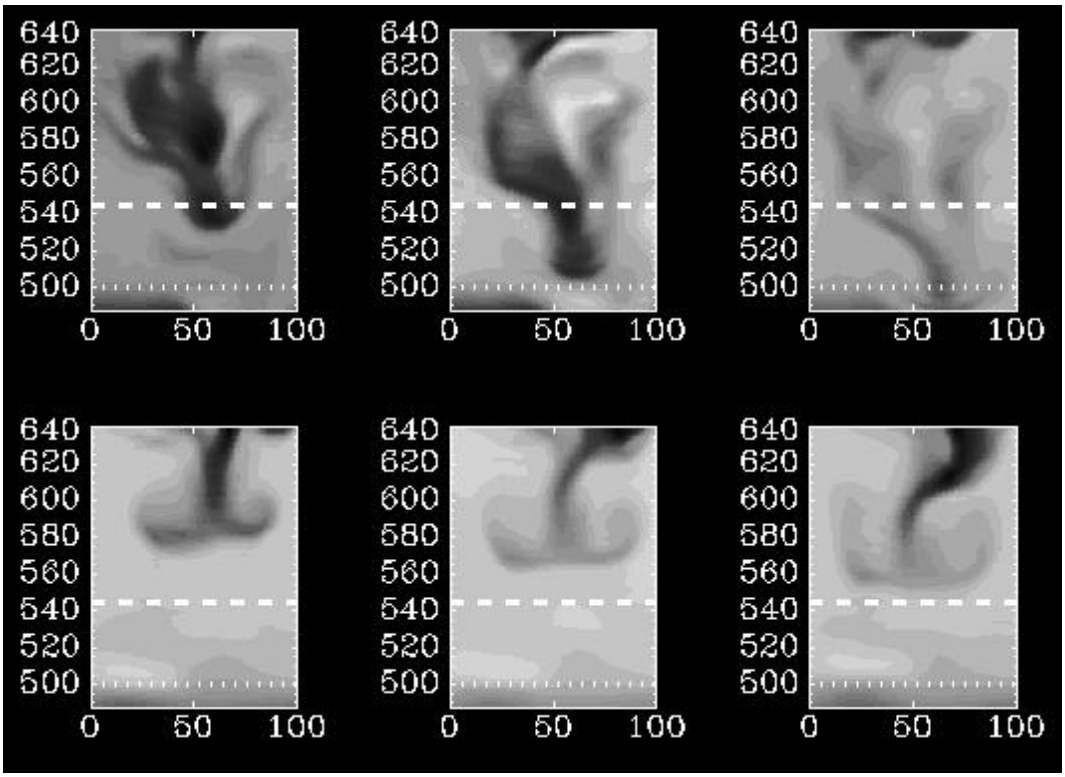

Figure 4: Evolution of two downdrafts shown as vertical slices of the entropy. Dark means low entropy.

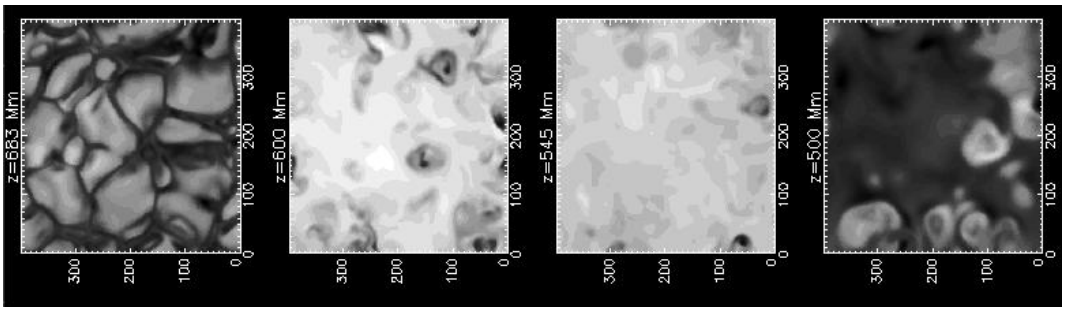

Figure 5: Horizontal slices of the temperature through a downdraft.

this "surface layer" does not correspond to the real surface of the sun which is still further up in the atmosphere. In the bulk of the convection zone ($z = 600\,\mathrm{Mm}$ and $z = 545\,\mathrm{Mm}$) the temperature pattern is rather different with cool regions now being disconnected. In the lower overshoot later the situation is different again. Even at the top of the overshoot layer ($z = 500\,\mathrm{Mm}$) there are now warm isolated spots. They are a consequence of cool downdrafts that shoot into the stable layer, where they appear hot in comparison to the surroundings, whose entropy decreases rapidly with depth (cf. Fig. 2).

5 The thermal time scale problem

In deeper layers of the sun the thermal time scale

$$\tau_{\rm th} = H_p^2/\chi = {\rm Pe}\ \tau_{\rm turnover} \tag{16}$$

becomes extremely long compared with the turnover time (Pe $\approx 10^7$). Using Eq. (6), $\tau_{\rm th}$ may also be written

$$\tau_{\rm th} = \frac{\rho c_p T H_p}{KT/H_p} \approx \frac{E_{\rm thermal}}{F_{\rm rad}} \tag{17}$$

where $E_{\rm thermal}$ is the thermal energy content and $F_{\rm rad}$ is the radiative flux. Near the bottom of the convection zone this is nearly the same as the local Kelvin-Helmholtz time scale

$$\tau_{\rm KH} = \frac{E_{\rm thermal}}{F_{\rm tot}}, \tag{18}$$

but in the bulk of the solar CZ and at the top, $\tau_{\rm KH}$ is much smaller than $\tau_{\rm th}$, because $F_{\rm rad}$ is tiny in comparison to $F_{\rm tot}$. When discussing thermal relaxation of simulations of deep solar convection, it is really $\tau_{\rm KH}$ rather than $\tau_{\rm th}$ that is relevant, but since the two are similar in the bottom layers, where thermal relaxation is the biggest problem, we continue to use $\tau_{\rm th}$ in the discussion below.

Note that $\tau_{\rm KH}$ varies by about eight orders of magnitude between the top and the bottom of the convection zone. On the other hand, the turnover time varies by only three orders of magnitude.

Table 1: Typical orders of magnitude of radiative diffusion χ, pressure scale height H_p, turbulent velocity u_t, as well as dynamical, thermal and Kelvin-Helmholtz time scales, respectively, at two different depths (cgs units).

location	r/R	χ	H_p	u_t	$\tau_{\rm th}$	$\tau_{\rm KH}$	$\tau_{\rm turnover}$
surface	1.0	10^{12}	10^8	10^5	10^8	10^5	10^3
bulk of CZ	0.8	10^7	10^{10}	10^4	10^{13}	10^{13}	10^6

The increasing gap between thermal and turnover time scales in deeper layers has important consequences for the evolution of the flow. Any perturbation will take a time much longer than the turnover time to relax. The problem of the thermal relaxation of simulations covering deeper parts of the solar convection zone was first pointed out by Chan & Sofia (1986). One may think that by setting up an initial state sufficiently close to the final one the relaxation time may be reduced, but this does not seem particularly helpful in practice. There is always a little perturbation in the initial state, which still takes a long time to relax. Faster relaxation could be achieved using for example an implicit or semi-implicit scheme (Fox 1994) that allows a longer time step, or by just using lower resolution, but again the danger is that a new and time consuming relaxation process will be necessary when switching back to a shorter time step or to higher resolution. Furthermore, any changes in the physics of the simulation (e.g. adding magnetic fields or rotation) may result in a new long relaxation period.

One may then ask the question how the results change if one brings the thermal and turnover times closer together. The ratio between thermal and dynamical (or turnover) time

scales is $\sim \mathrm{Pe} \approx (F_{\rm conv}/F_{\rm rad})\ (T/\delta T)$; see Eq. (9). In order to simplify the discussion, we consider the scaling of the Peclet number near the bottom of the convection zone, where $F_{\rm conv} \sim F_{\rm rad} \sim F$. The scaling may be expressed either in terms of the total flux F, or in terms of the product of the Rayleigh and Prandtl numbers RaPr.

The scaling of the relative temperature fluctuation may be obtained from considering the convective flux $F_{\rm conv}$, that is proportional to the product $u_t \delta T$, and the kinetic energy per unit mass u_t^2, that is proportional to δT (buoyancy), so

$$F_{\rm conv} \sim u_t^3 \sim \delta T^{3/2} \tag{19}$$

The relation to the Rayleigh and Prandtl numbers may be obtained by observing that the radiative flux $F_{\rm rad}$ is proportional to χ, so the product RaPr ($\sim \chi^{-2}$) is proportional to $F_{\rm rad}^{-2}$. Since $F_{\rm conv} \sim F_{\rm rad} \sim F$ in the layer we are considering, we obtain

$$\tau_{\rm th}/\tau_{\rm turnover} \sim \mathrm{Pe} \sim (\mathrm{RaPr})^{1/3} \sim F^{-2/3} \tag{20}$$

Thus, in order to bring the thermal and dynamical time scales closer together, one must increase the total flux or, equivalently, lower the Rayleigh number. The fact that the flux decreases with increasing Rayleigh number may appear counterintuitive, but is because a reduced radiative diffusivity corresponds to a reduced radiative energy flux.

Thus, the significance of increasing the Rayleigh number in numerical experiments is not just to lower the viscosity and diffusivity, but also to lower the total flux and thus bring the thermal time scale closer to that of the real system.

Table 2: Mach number, flux (relative to the solar value), and Peclet number for different values of the Rayleigh number (or rather the product RaPr). The degree of feasibility in subjective terms is also indicated.

RaPr	Ma	$F/F_\odot$	Pe	feasibility
10^6	10^{-1}	10^9	10	"trivial"
10^{12}	10^{-2}	10^6	10^3	feasible
10^{18}	10^{-3}	10^3	10^5	not feasible
10^{24}	10^{-4}	1	10^7	the sun

In Table 2 we have listed some relevant parameters for a few cases. From this we see that currently feasible models must have a flux that is of the order of a million times the solar flux, in order to avoid the problem with the thermal relaxation time scale. Such "toy models" may still be quite useful, because they display qualitative features that may also be expected to appear in models with lower fluxes (and ultimately in the real thing). To the extent that one can understand and derive the scaling of these features with total flux, the toy models still serve a useful purpose.

Some features may be expected to be difficult to find scaling relations for. For example, the extent of the overshoot layer will be too large in the toy models and the braking of overshooting bubbles has a strongly nonlinear dependence on the overshooting distance. The extent of the overshoot layer could be reduced by making the subadiabatic gradient steeper, but this requires modifying the opacity law.

The main moral of all this is that it is currently impractical to model solar convection in deeper layers using realistic fluxes. Instead, we must rely on toy models with excess flux, i.e.

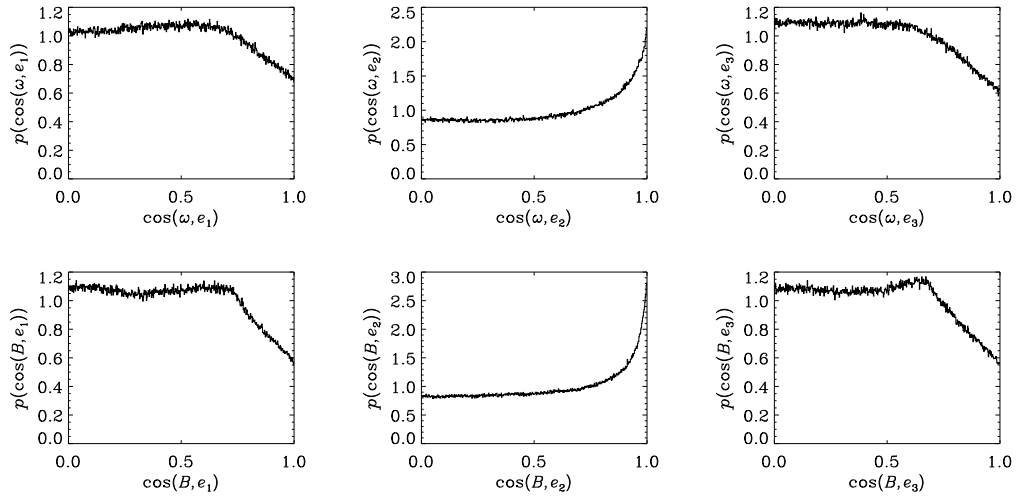

Figure 6: Upper row: histograms of the cosines of the angles between $\boldsymbol{\omega}$ and the three eigenvectors $\boldsymbol{e}_1$, $\boldsymbol{e}_2$, $\boldsymbol{e}_3$, of the rate of strain matrix. Lower row: same, as upper row, but for $\boldsymbol{B}$. The direction of compression corresponds to $\boldsymbol{e}_1$ and the direction of stretching to $\boldsymbol{e}_3$. Note the enhanced probability of the intermediate eigenvector $\boldsymbol{e}_2$ to be aligned with $\boldsymbol{\omega}$ or $\boldsymbol{B}$.

with values of $F/F_\odot$ significantly larger than unity, and try to understand the model output as $F/F_\odot$ approaches the solar value. The scaling relations discussed here should be tested and deviations be understood in terms of the specific physical processes involved.

6 The formation of magnetic structures

In the sun the gas is hot enough to be ionized in the bulk of the convection zone, so it is electrically conducting. Consequently, the Maxwell equations are then coupled to the fluid equations via the Lorentz force and Ohm's law. It is generally found that turbulent convection can lead to dynamo action (e.g. Gilman 1983, Glatzmaier 1985, Meneguzzi & Pouquet 1989), which is the self-excited (spontaneous) conversion of kinetic energy into magnetic energy. Although this process is actually central to some of our work we are going to quote below, we only want to discuss those aspects that are of somewhat wider interest. Important aspects concern the formation and advection of magnetic structures. This is generally relevant, because magnetic fields behave in many ways similar to vorticity.

In ordinary nonmagnetic turbulence the flow consists of a large number of vortex tubes (Siggia 1981, Kerr 1985, Vincent & Meneguzzi 1991). Something similar happens with the magnetic field, at least when the field is developing freely and not imposed externally. In the inviscid hydrodynamical case the vorticity occurs rather in the form of sheets (Cao et al. 1996). In the magnetic case the situation is not quite clear yet. Visualisations of the strongest $\boldsymbol{B}$-vectors suggests mostly tube-like structures (Nordlund et al. 1992), although sometimes sheets can also be found. A multifractal analysis of the data also suggests that the strongest flux concentrations have the form of tubes (Brandenburg et al. 1992). However, the structure function exponents in MHD turbulence can best be understood using a model

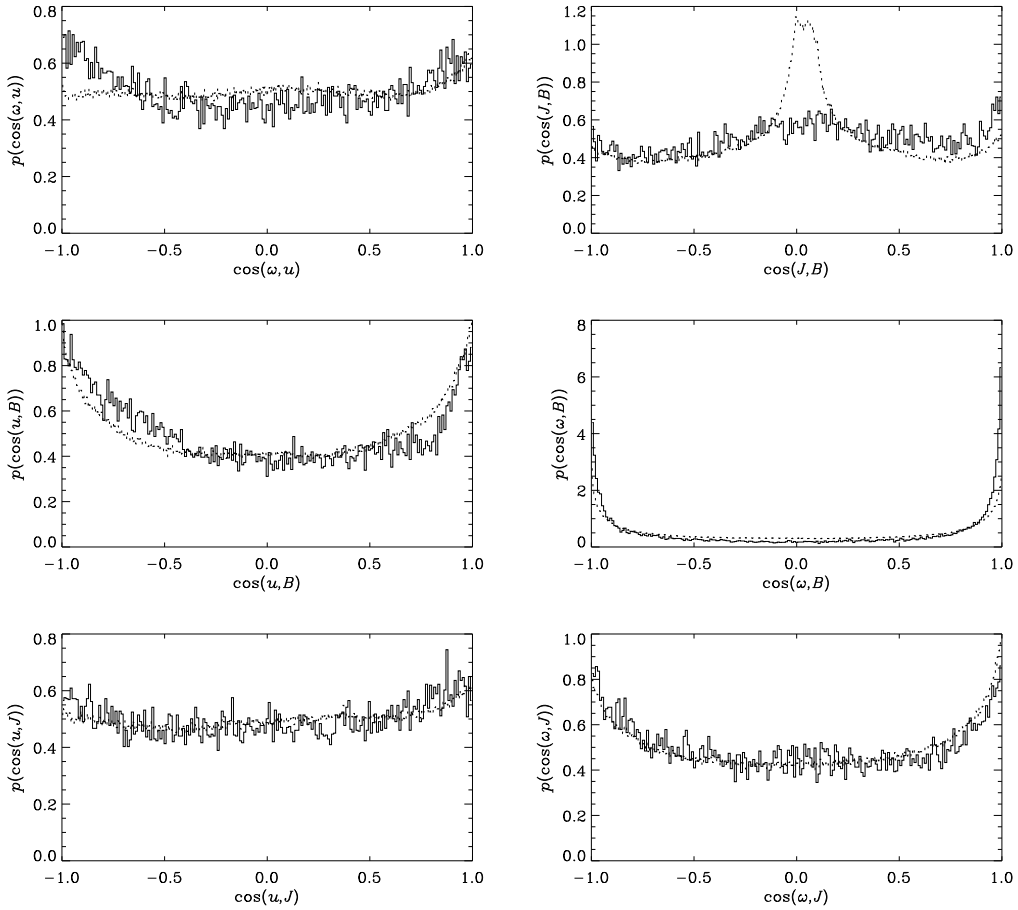

Figure 7: Cosines of the angles between different vector fields in the simulation. Note especially the strong tendency for alignment (or anti-alignment) between between the vorticity $\boldsymbol{\omega}$ and the magnetic field $\boldsymbol{B}$. The dotted lines refer to all points in a snapshot and the solid lines only to those where the magnetic field exceeds its root mean square value by a factor of three.

that assumes sheet-like structures (Politano & Pouquet 1995).

In hydrodynamical turbulence the vortex tubes are aligned with the individual vorticity vectors $\boldsymbol{\omega}$. Likewise, in MHD turbulence the magnetic flux tubes are aligned with the individual magnetic field vectors $\boldsymbol{B}$. In both cases the tendency for alignment is thought to be a diffusive phenomenon (Constantin et al. 1995, Brandenburg et al. 1995a). In ordinary turbulence the vortex tubes are aligned with the intermediate eigenvector of the rate of strain matrix. The same is true of the magnetic field which is mostly parallel to the intermediate eigenvector (Fig. 6). It is then not surprising that the vorticity and magnetic field vectors are mostly parallel to each other (Fig. 7). There is also a tendency for $\boldsymbol{u}$ and $\boldsymbol{B}$ to be aligned, but this effect is quite weak in comparison with the enhanced alignment of $\boldsymbol{\omega}$ and $\boldsymbol{B}$. In the plot we have distinguished between all data points in the simulations (dotted lines) and

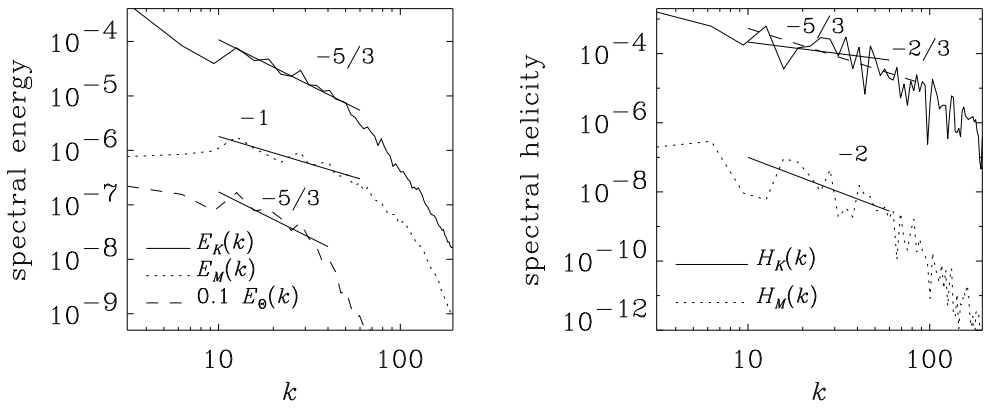

Figure 8: Left panel: power spectra of the kinetic energy (solid line), magnetic energy (dotted line) and temperature fluctuation (dashed line). Right panel: power spectra of the kinetic and magnetic helicities, $H_K(k)$ and $H_M(k)$, respectively.

those where the field is strong (solid line). The correlation plot of $\boldsymbol{J}$ and $\boldsymbol{B}$ indicated that the two vectors tend to be perpendicular on average (dotted line), but this is no longer true of those regions where the field is strong (solid line). Details of this analysis can be found in Brandenburg et al. (1996).

Nevertheless, despite their similarity, in other respects the magnetic field and the vorticity are actually quite different. The powerspectrum of the velocity has a short range roughly like a Kolmogorov $k^{-5/3}$ spectrum, so the vorticity has a $k^{+1/3}$ spectrum. However, a similar spectrum is not observed for the magnetic field, except very early in the evolution when nonlinear effects were still unimportant (Brandenburg et al. 1996).

7 Magnetic dynamo action

Video animations of the strong magnetic field vectors show how magnetic flux tubes evolve. Some snapshots of such animations are reproduced in Fig. 9. One sees a tendency for magnetic loops to fold onto themselves. This appears to be similar to the stretch-twist-fold dynamo of Vainshtein & Zeldovich (1972), (see also a recent monograph by Childress & Gilbert 1995). In this type of dynamo constructive folding of tubes enhances the flux. Whether or not this is really the dominant process in the simulations remains to be seen. It is clear, however, that there is a dynamo acting in the simulations: magnetic energy increases exponentially in time over many orders of magnitude until saturation sets in (Fig. 10). For further details see Nordlund et al. (1992) and Brandenburg et al. (1996). After some period of exponential growth two solutions with different initial conditions settle at the same value. During the growth phase the size of magnetic structures, as measured by the magnetic Taylor microscale,

$$\lambda_M = \sqrt{5\langle \boldsymbol{B}^2 \rangle / \langle (\boldsymbol{\nabla} \times \boldsymbol{B})^2 \rangle}, \tag{21}$$

increase with time. This suggests that the magnetic structures are intensifying not just by stretching, but in particular by growing in thickness, possibly via folding.

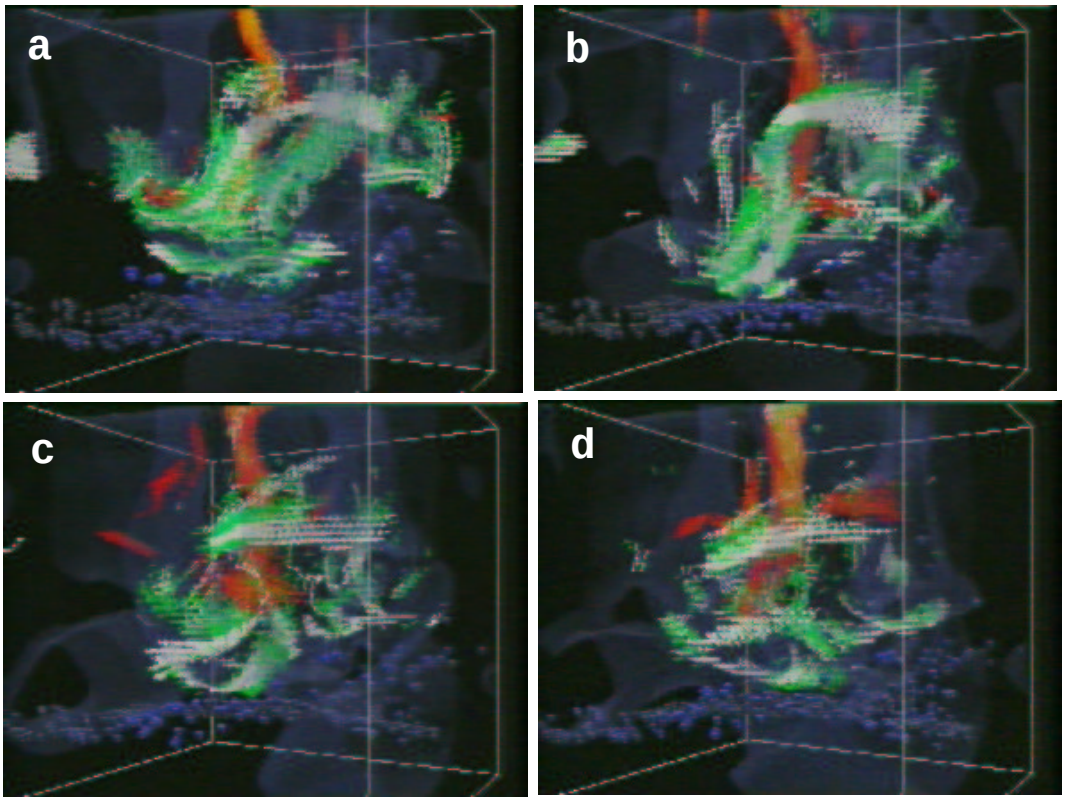

Figure 9: Snapshots of a video animation showing a strong magnetic flux tube (white) being wrapped around a spinning downdraft (dark grey, extending from the top of the box to the middle). As time goes on (frames a-d) the magnetic flux loop appears to be folded onto itself and is being pushed further down to the bottom the convection zone and into the lower overshoot layer (lower half of the box).

8 Downward pumping

In the presence of rotation and stratification there is a pronounced phenomenon of downward "pumping" of magnetic fields and vorticity. This is seen in images of the magnetic energy density $\boldsymbol{B}^2$ (Fig. 11) and the enstrophy density $\boldsymbol{\omega}^2$ (Fig. 12), showing that most of the field and vorticity accumulates near the lower overshoot layer. This is also clearly seen in video animations of the magnetic field, as described by Nordlund et al. (1992) and Brandenburg et al. (1996), see also Fig. 9. The amount of vorticity and magnetic field that has been pumped downwards is however much weaker if there is no rotation (Fig. 13). In that case most of the vorticity is seen near the top where fluid overturns into the downdraft lanes.

The nature of this pumping effect is not fully clarified. There are two forms of pumping that have been discussed in the context of magnetic fields. One is topological pumping of a horizontal magnetic field by convection in a connected network of downward or upward motion. The other is turbulent pumping. The two mechanism are quite distinct, but easily confused because both start with 't'. (See Brandenburg et al. 1995c for references and a recent discussion of the two effects.) In our simulations with rotation the pumping cannot be

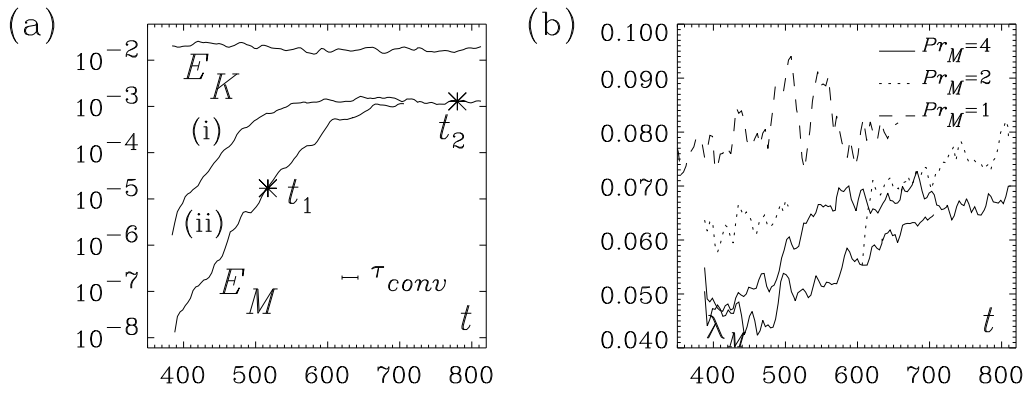

Figure 10: Left: evolution of the magnetic energy E_K and kinetic energy E_K for two different runs. Right: evolution of the magnetic Taylor microscale for different magnetic Prandtl numbers Pr_M.

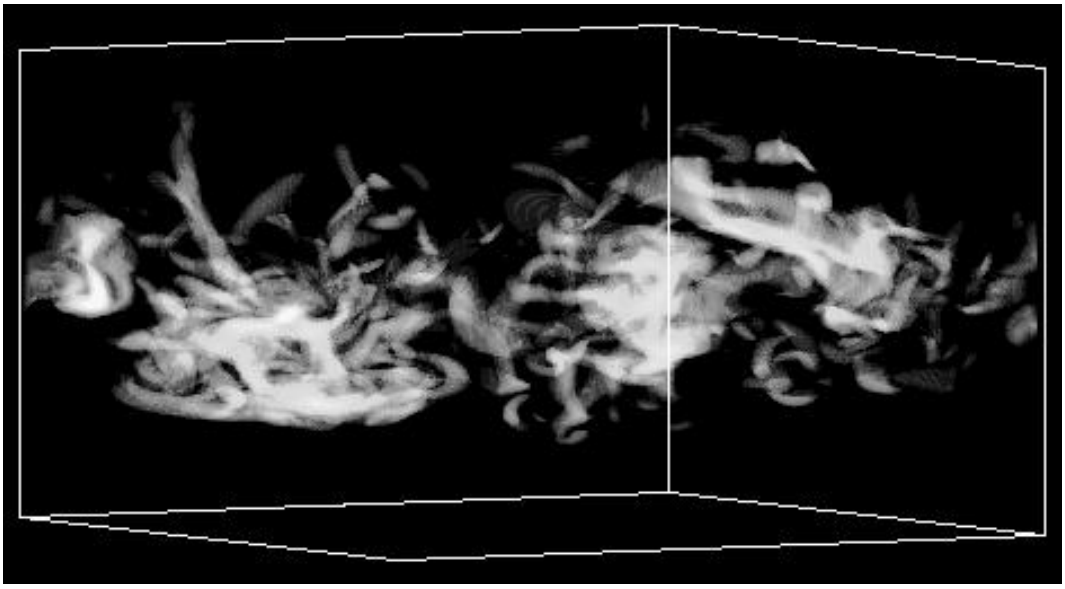

Figure 11: Three-dimensional image of the magnetic energy density $\boldsymbol{B}^2$. Note that most of the magnetic field is near the lower overshoot layer, which is located just a little below the middle of the box.

topological, because the downdrafts do not form a connected network. Turbulent pumping remains a possibility, but the details of the actual mechanism must be different from the original turbulent pumping, which corresponds to a net transport velocity $\boldsymbol{u}_{\rm pump} = -\frac{1}{2}\boldsymbol{\nabla}\eta_t$, where $\eta_t \sim \frac{1}{3}u_t\ell$ is the standard expression for the turbulent magnetic diffusivity, where ℓ is the correlation length of the turbulence. This expression involves just ℓ and u_t, which is

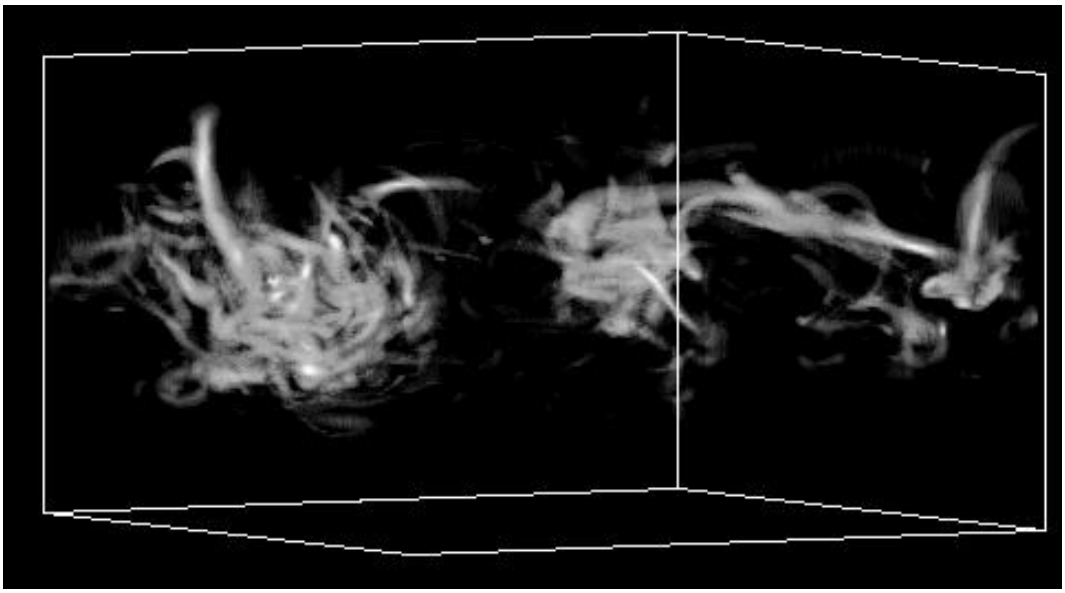

Figure 12: Three-dimensional image of the enstrophy density $\boldsymbol{\omega}^2$. Similar to Fig. 11 most of the vorticity is near the lower overshoot layer.

independent of rotation, so this expression is too simplistic in describing our results.

9 Outstanding problems

In the last three sections we have touched upon some aspects of magnetic field evolution in solar convection. This poses indeed a challenging problem. Among other reasons, we need to study solar magnetism in order to understand variations of the solar luminosity which, in turn, can influence the earth's climate.

A particularly important problem is to understand the origin of the large scale magnetic field and its 11 years cyclic variations (i.e. the sunspot cycle). Simulations are currently under way to investigate the effect of shear on a convective dynamo. Promising results have emerged in the context of accretion disc turbulence simulations where strong shear leads to a cyclic large scale magnetic field (Brandenburg et al. 1995b). In this case the magnetic field evolution is governed by flows that result from the magnetic field itself due to an instability. In the case of accretion discs relevant instabilities include the magnetic shear and buoyancy instabilities (for a review see Schramkowski & Torkelsson 1996). The same idea may also apply to stars where, in addition to magnetic buoyancy and shear instabilities, destabilized magnetostrophic waves have been discussed (Schmitt 1985). There is a related approach based on the Parker and other magnetic instabilities of flux tubes by Ferriz-Mas, Schmitt & Schüssler (1994). More recently, similar investigations have been carried out in connection with the dynamo effect in galaxies (Hanasz & Lesch 1997).

Future simulations will hopefully reveal whether the large scale field of the sun is really governed by magnetic instabilities, or whether cyclonic convection alone can do the job. An important prerequisite of realistic models of solar convection and magnetic field generation are high Rayleigh numbers and small fluxes. We hope that significant progress can be made

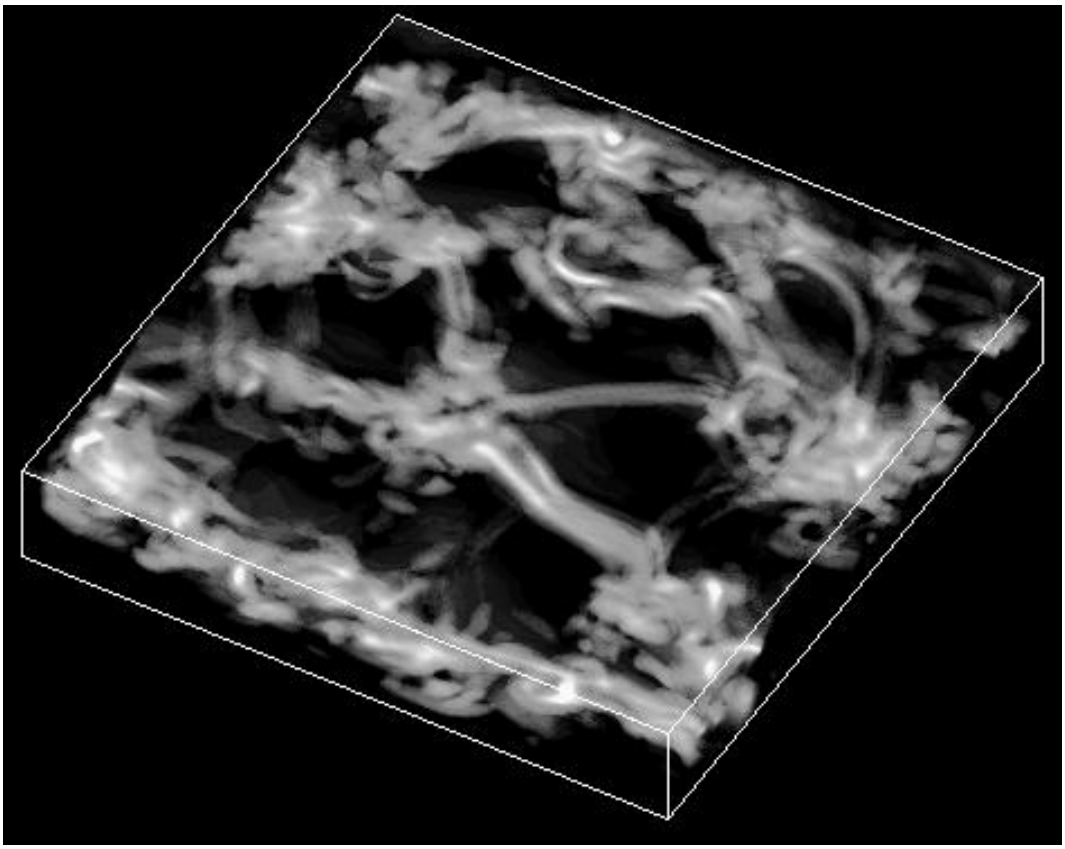

Figure 13: Three-dimensional visualisation of the vorticity in a simulation without rotation.

in addressing these issues in the near future.

References

Brandenburg, A., Procaccia, I., Segel, D., Vincent, A., "Fractal level sets and multifractal fields in direct simulations of turbulence," *Phys. Rev.* **A 46**, 4819-4828 (1992).

Brandenburg, A., Procaccia, I., Segel, D., "The size and dynamics of magnetic flux structures in MHD turbulence," *Phys. Plasmas* **2**, 1148-1156 (1995a).

Brandenburg, A., Nordlund, Å., Stein, R. F., Torkelsson, U., "Dynamo generated turbulence and large scale magnetic fields in a Keplerian shear flow," *Astrophys. J.* **446**, 741-754 (1995b).

Brandenburg, A., Moss, D., Shukurov, A., "Galactic fountains as magnetic pumps," *Monthly Notices Roy. Astron. Soc.* **276**, 651-662 (1995c).

Brandenburg, A., Jennings, R. L., Nordlund, Å., Rieutord, M., Stein, R. F., Tuominen, I., "Magnetic structures in a dynamo simulation," *J. Fluid Mech.* **306**, 325-352 (1996).

Bray, R.J., Loughhead, R.E., Durrant, C.J. *The solar granulation*, Cambridge University

Press (1984).

Brummel, N. H., Hurlburt, N. E., & Toomre, J., "Turbulent compressible convection with rotation. I. Flow structure and evolution," *Astrophys. J.* **473**, 494-513 (1996).

Cao, N. Z., Chen, S. Y., & She, Z. S., "Scalings and relative scalings in the Navier-Stokes turbulence," *Phys. Rev. Letters* **76**, 3711-3714 (1996).

Chandrasekhar, S. *Hydrodynamic and Hydromagnetic Stability.* Oxford, Clarendon Press (1961). Dover Publications, Inc., New York

Chan, K. L., Sofia, S., "Turbulent compressible convection in a deep atmosphere. III. Tests on the validity and limitation of the numerical approach," *Astrophys. J.* **307**, 222-241 (1986).

Childress, S. & Gilbert, A. G. *Stretch, twist, fold: the fast dynamo.* Berlin: Springer (1995).

Constantin, P., Procaccia, I. & Segel, D., "Creation and dynamics of vortex tubes in 3-dimensional turbulence," *Phys. Rev.* **E**, 3207-3222 (1995).

Ferriz-Mas, A., Schmitt, D., Schüssler, M., "A dynamo effect due to instability of magnetic flux tubes," *Astron. Astrophys.* **289**, 949-949 (1994).

Fox, P. private communication (1994).

Frank, J., King, A. R., & Raine, D. J. *Accretion power in astrophysics.* Cambridge: Cambridge Univ. Press (1992).

Galsgaard, K. & Nordlund, Å., "Heating and activity of the solar corona: I. boundary shearing of an initially homogeneous magnetic-field," *J. Geophys. Res.* **101**, 13445-13460 (1996).

Gilman, P. A., "Dynamically consistent nonlinear dynamos driven by convection in a rotating spherical shell. II. Dynamos with cycles and strong feedbacks," *Astrophys. J. Suppl.* **53**, 243-268 (1983).

Glatzmaier, G. A., "Numerical simulations of stellar convective dynamos. II. Field propagation in the convection zone," *Astrophys. J.* **291**, 300-307 (1985).

Hanasz, M. & Lesch, H., "The galactic dynamo effect due to Parker-shearing instability of magnetic flux tubes. I. General formalism and the linear approximation," *Astron. Astrophys.,* in press (1997). astro-ph/9610167

Kerr, R. M., "Higher-order derivative correlations and the alignment of small-scale structures in isotropic numerical turbulence," *J. Fluid Mech.* **153**, 31-58 (1985).

Kippenhahn, R. & Weigert, A. *Stellar structure and evolution.* Springer: Berlin (1990).

Kolmogorov, A. N., "The local structure of turbulence in incompressible viscous fluid for very large Reynolds numbers," *CR Acad. Sci. USSR* **30**, 299-303 (1941).

Meneguzzi, M., Pouquet, A., "Turbulent dynamos driven by convection," *J. Fluid Mech.* **205**, 297-312 (1989).

Nordlund, Å., Brandenburg, A., Jennings, R. L., Rieutord, M., Ruokolainen, J., Stein, R. F., Tuominen, I., "Dynamo action in stratified convection with overshoot," *Astrophys. J.* **392**, 647-652 (1992).

Nordlund, Å., Stein, R. F., Brandenburg, A., "Supercomputer windows into the solar convection zone," *Bull. Astr. Soc. India* **24**, 261-279 (1996).

Politano, H. & Pouquet, A., "Model of intermittency in magnetohydrodynamic turbulence," *Phys. Rev.* **E 52**, 636-641 (1995).

Ruzmaikin, A. A., Sokoloff, D. D. & Shukurov, A. M. *Magnetic Fields of Galaxies.* Kluwer, Dordrecht (1988).

Schmitt, D. *Dynamowirkung magnetostrophischer Wellen.* PhD dissertation (1985).

Schramkowski, G. P. & Torkelsson, U., "Magnetohydrodynamic instabilities and turbulence in accretion disks," *Astron. Astrophys. Rev.* **7**, 55-96 (1996).

Siggia, E. D., "Numerical study of small-scale intermittency in three-dimensional turbulence," *J. Fluid Mech.* **107**, 375-406 (1981).

Stein, R.F., Nordlund, Å., "Topology of convection beneath the solar surface," *Astrophys. J. Letters* **342**, L95-L98 (1989).

Thompson, C. & Duncan, R. C., "Neutron star dynamos and the origins of pulsar magnetism," *Astrophys. J.* **408**, 194-217 (1993).

Vainshtein, S. I. & Zeldovich, Ya. B., "Origin of magnetic fields in astrophysics," *Sov. Phys. Usp.* **15**, 159-172 (1972).

Vincent, A. & Meneguzzi, M., "The spatial structure and statistical properties of homogeneous turbulence," *J. Fluid Mech.* **225**, 1-20 (1991).